A finite element analysis for the mixed mode crack growth in a viscoelastic and orthotropic medium

Rostand Moutou Pitti, F. Dubois, O. Pop, Joseph Absi

International Journal of Solids and Structures 46 (2009) 3548–3555

Contents lists available at ScienceDirect

International Journal of Solids and Structures

journal homepage: www.elsevier.com/locate/ijsolstr

A finite element analysis for the mixed mode crack growth in a viscoelastic and orthotropic medium

R. Moutou Pitti *, F. Dubois, O. Pop, J. Absi

Groupe d'Etude des Matériaux Hétérogènes – Civil Engineer and Durability, Limoges University, Centre Universitaire Génie Civil d'Egletons, 19300 Egletons, France

ARTICLE INFO

Article history:
Received 4 June 2008
Received in revised form 25 April 2009
Available online 14 June 2009

Keywords:
Fracture mechanics
Creep
Mixed-mode crack
Finite element
Conservation integral

ABSTRACT

This paper deals with a finite element algorithm for the creep crack growth process in a viscoelastic medium. The main developments focus on the coupling between the *M*-integral and an incremental formulation for the viscoelastic behavior. In this context, mixed mode configurations are simulated for orthotropic symmetries. An algorithm uncoupling viscoelastic incremental formulation and the fracture procedure is resolved with finite element software. The global approach is validated in terms of the evolution of energy release rate versus time and the advance of cracks. Numerical simulations are based on a Constant Tension Shear model. The insensitivity of the *M*-integral to the integration domain is shown from creep crack growth simulations for mixed mode configurations.

1. Introduction

Many composite materials are subjected to mixed-mode crack growth development induced by complex processes over a long period (Bian and Lim, 2007). These different observations are increased when their anisotropic and orthotropic character combine with the viscoelastic behavior (Barbero and Luciano, 1995; Cortés and Elejabarrieta, 2006) of these materials. Therefore, several investigations, based on numerical and analytical approaches, have been performed in fracture mechanics. Among them, Tenchev and Falzon (2007) have proposed analytic solutions for wood specimens loaded in the mixed-mode. Sun and Qian (1997), Vasic et al. (2005) and Ratnesh and Chandra Kishen (2008) have used numerical methods for the study of fracture mechanics properties. Also, Moutou Pitti et al. (2007a) have proposed a numerical and analytical model adapted to separating mixed modes in the viscoelastic case, but this tool is limited to static cracking. Consequently, in order to exactly translate the real effects described previously, the development of new methods is required.

Using the *M*-integral approach, we develop a method for separating mixed-mode fractures in viscoelastic media during the creep crack growth process. The *M*-integral approach was initially proposed by Chen and Shield (1977) and is based on conservation laws (Noether, 1971). Moutou Pitti et al. (2007a) have adapted this form to viscoelastic material with a bilinear form of the Helmholtz strain energy density $F^{\bullet}$. In order to model time dependent crack growth processes in materials, he has generalized this method to viscoelastic behavior (Moutou Pitti et al., 2006; Moutou Pitti et al., 2007b). In this paper, this third approach is implemented and solved using the finite element method.

The analytical and modeling expressions of the *M*-integral method are proposed in the first section. According to a generalized Kelvin Voigt model, this integral is adapted to viscoelastic behavior in the second part. Also, the viscoelastic energy release rate is deduced through the stress intensity factor using the *M* approach. In the third section, an incremental viscoelastic formulation and a fracture algorithm are used in order to implement analytical tools in a finite element process. In the numerical process, the mixed-mode ratio is introduced by the application of a modified CTS (Constant Tension Shear) specimen. This specimen has been initially developed by Richard (1981) and Richard and Benitz (1983) so as to generate mixed-mode ratios in isotropic materials, and it was adapted to orthotropic media by Valentin and Caumes (1989). In the last section, the variations of energy release rate versus time and crack length are shown in mixed-mode configurations for different path integrations.

2. Invariant integrals

2.1. M-integral

In linear elastic materials, the energy release rate is generally computed with Rice's *J*-integral (Rice, 1968). In order to separate fracture modes, Chen and Shield (1977) first proposed the *M*-integral based on a *J*-integral concept. This *M* approach is based on a

* Corresponding author. Tel.: +33 555 934 535; fax: +33 555 934 531.
E-mail address: rostandpitti@yahoo.fr (R. Moutou Pitti).

0020-7683/$ - see front matter © 2009 Elsevier Ltd. All rights reserved.
doi:10.1016/j.ijsolstr.2009.05.020

conservation law (Noether, 1971) applied in an Arbitrary Lagrangian Eulerian (ALE) configuration (Moutou Pitti et al., 2007a; Dubois et al., 1999). Moutou Pitti et al. (2006, 2007b) have developed a generalized M-integral form that is adapted to viscoelastic orthotropic materials during the crack growth process. Without pressure on the crack lips, the new expression of the M-integral is given by:

$$M=\int_{\Gamma_1}\left(F^{\bullet}\cdot n_1-\left(\frac{\partial F^{\bullet}}{\partial u_{i,j}}\cdot u_{i,1}+\frac{\partial F^{\bullet}}{\partial v_{i,j}}\cdot v_{i,1}\right)\cdot n_j\right)\mathrm{d}\Gamma_1 + \int_{A(\Gamma_1)}\left(\left(\frac{\partial F^{\bullet}}{\partial u_{i,\alpha}}\delta u_{i,1}\right)_{,\alpha}+\left(\frac{\partial F^{\bullet}}{\partial v_{i,\alpha}}\delta v_{i,1}\right)_{,\alpha}-\left(F^{\bullet}_{,1}(u)\right)+F^{\bullet}_{,1}(v)\right)\mathrm{d}V. \tag{1}$$

Here, $\alpha(x_1,x_2,t)$ is a spatial and temporal function, n_j are the components of the normal vector $\vec{n}$ of the curvilinear integration domain Γ_1, and $A(\Gamma_1)$ designates the area enclosed by Γ_1 (Fig. 1). u and v are real and virtual displacement fields, respectively. The virtual displacement v is given according to Sih's (1974) singular form:

$$v_1=2\cdot {}^{v}K_1\cdot\sqrt{\frac{r}{2\cdot\pi}}\cdot\Re\left[\frac{1}{s_1-s_2}\cdot\left(p_2\cdot s_1\cdot\rho_2^{0.5}-p_1\cdot s_2\cdot\rho_1^{0.5}\right)\right] + 2\cdot {}^{v}K_2\cdot\sqrt{\frac{r}{2\cdot\pi}}\cdot\Re\left[\frac{1}{s_1-s_2}\cdot\left(p_2\cdot\rho_2^{0.5}-p_1\cdot\rho_1^{0.5}\right)\right]$$

$$v_2=2\cdot {}^{v}K_1\cdot\sqrt{\frac{r}{2\cdot\pi}}\cdot\Re\left[\frac{1}{s_1-s_2}\cdot\left(q_2\cdot s_1\cdot\rho_2^{0.5}-q_1\cdot s_2\cdot\rho_1^{0.5}\right)\right] + 2\cdot {}^{v}K_2\cdot\sqrt{\frac{r}{2\cdot\pi}}\cdot\Re\left[\frac{1}{s_1-s_2}\cdot\left(q_2\cdot\rho_2^{0.5}-q_1\cdot\rho_1^{0.5}\right)\right] \tag{2}$$

$$\text{with } \rho_j=\cos(\varphi)+i\cdot s_j\cdot\sin(\varphi), j\in\{1;2\} \tag{3}$$

$$\text{and } p_j=S_{11}\cdot s_j^2+S_{12};q_j=\frac{S_{22}}{s_j}+S_{12}\cdot s_j. \tag{4}$$

s_1 and s_2 are the roots of the classical characteristic equation given by Airy's representation:

$$S_{11}\cdot s_j^4+(2\cdot S_{12}+S_{33})\cdot s_j^2+S_{22}=0. \tag{5}$$

$S_{11},S_{12},S_{22},S_{33}$ indicate components of the compliance tensor according to an orthotropic symmetry for plane stress assumptions. ${}^{v}K_{\beta}(\beta\in\{1,2\})$ are virtual stress intensity factors in opening and shear mode, respectively. r and φ are the ordinary polar coordinates in a reference frame centered at the crack tip. $F^{\bullet}$ is a bilinear form of the strain elastic energy defined by Chen and Shield (1977) in these terms:

$$\frac{\partial F^{\bullet}}{\partial u_{i,j}}=\frac{1}{2}\sigma_{ij}^{(v)}\ \text{and}\ \frac{\partial F^{\bullet}}{\partial v_{i,j}}=\frac{1}{2}\sigma_{ij}^{(u)}. \tag{6}$$

Introducing the bilinear form (6) in expression (1), we obtain:

$$M=\frac{1}{2}\int_{\Gamma_1}\left(\sigma_{ij,1}^{(v)}\cdot u_i-\sigma_{ij}^{(u)}\cdot v_{i,j}\right)\cdot n_j\mathrm{d}\Gamma_1+\frac{1}{2}\int_{A(\Gamma_1)}\left(\left(\sigma_{ij}^{(v)}\cdot(u_{i,j})_{,1}+\sigma_{ij}^{(u)}\cdot(v_{i,j})_{,1}\right)-\left(\left(\sigma_{ij}^{(v)}\cdot u_{i,j}\right)_{,1}+\left(\sigma_{ij}^{(u)}\cdot v_{i,j}\right)_{,1}\right)\right)\mathrm{d}V, \tag{7}$$

in which $\sigma_{ij}^{(v)}$ and $\sigma_{ij}^{(u)}$ are virtual and real stresses, respectively.

2.2. $M\theta$ integral

The expression of interest is defined on the curvilinear integration contour Γ_1. In order to evaluate the M-integral with a finite element method using a displacement approach, the surface domain is preferred. This problem is solved by introducing a vector field $\vec{\theta}$ (Destuynder et al., 1983) ($\theta_1=1$ and $\theta_2=0$ inside the ring, $\vec{\theta}=\vec{0}$ outside it, Fig. 2).

Let us now consider the following expression:

$$\dot{p}_{j,k}=\frac{1}{2}\left(\sigma_{ij,k}^{(v)}\cdot u_i-\sigma_{ij}^{(u)}\cdot v_{i,k}\right). \tag{8}$$

Substituting expression (8) in (7), we obtain this third expression:

$$M\theta=\int_{\Gamma_1}\dot{p}_{j,k}\cdot n_j\cdot\theta_k\mathrm{d}\Gamma_1+\frac{1}{2}\int_{A(\Gamma_1)}\left(\left(\sigma_{ij}^{(v)}\cdot(u_{i,j})_{,k}+\sigma_{ij}^{(u)}\cdot(v_{i,j})_{,k}\right)-\left(\left(\sigma_{ij}^{(v)}\cdot u_{i,j}\right)_{,k}+\left(\sigma_{ij}^{(u)}\cdot v_{i,j}\right)_{,k}\right)\right)\cdot\theta_k\mathrm{d}V. \tag{9}$$

The application of Gauss–Ostrogradski's theorem to the first term of gives us:

$$M\theta=\int_V-(\dot{p}_{j,kj}\cdot\theta_k+\dot{p}_{j,k}\cdot n_j\cdot\theta_{k,j})\mathrm{d}V+\frac{1}{2}\int_{A(\Gamma_1)}\left(\left(\sigma_{ij}^{(v)}\cdot(u_{i,j})_{,k}+\sigma_{ij}^{(u)}\cdot(v_{i,j})_{,k}\right)-\left(\left(\sigma_{ij}^{(v)}\cdot u_{i,j}\right)_{,k}+\left(\sigma_{ij}^{(u)}\cdot v_{i,j}\right)_{,k}\right)\right)\cdot\theta_k\mathrm{d}V. \tag{10}$$

According to the insensitivity of the M-integral to the integration domain, $A(\Gamma_1)$ can be replaced by the difference between the total surface Ω and the crown surface V. Then, the second term of expression (10) can be rewritten as follows:

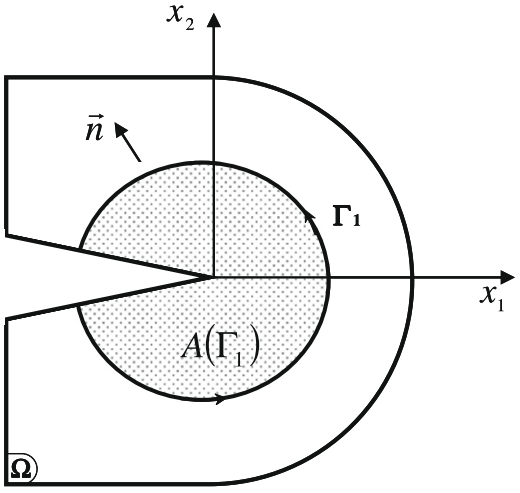

Fig. 1. Contour and area around the crack tip.

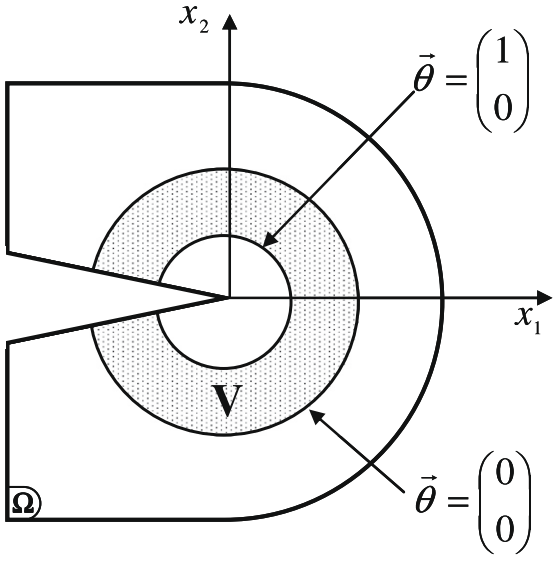

Fig. 2. Integration domain.

$$\frac{1}{2}\int_{A(\Gamma_1)}\left(\left(\sigma_{ij}^{(v)}\cdot(u_{i,j})_{,k}+\sigma_{ij}^{(u)}\cdot(v_{i,j})_{,k}\right)-\left(\left(\sigma_{ij}^{(v)}\cdot u_{i,j}\right)_{,k}+\left(\sigma_{ij}^{(u)}\cdot v_{i,j}\right)_{,k}\right)\right)\cdot\theta_k\mathrm{d}V=\frac{1}{2}\int_{\Omega}\left(\left(\sigma_{ij}^{(v)}\cdot(u_{i,j})_{,k}+\sigma_{ij}^{(u)}\cdot(v_{i,j})_{,k}\right)-\left(\left(\sigma_{ij}^{(v)}\cdot u_{i,j}\right)_{,k}+\left(\sigma_{ij}^{(u)}\cdot v_{i,j}\right)_{,k}\right)\right)\cdot\theta_k\mathrm{d}\Omega-\frac{1}{2}\int_{V}\left(\left(\sigma_{ij}^{(v)}\cdot(u_{i,j})_{,k}+\sigma_{ij}^{(u)}\cdot(v_{i,j})_{,k}\right)-\left(\left(\sigma_{ij}^{(v)}\cdot u_{i,j}\right)_{,k}+\left(\sigma_{ij}^{(u)}\cdot v_{i,j}\right)_{,k}\right)\right)\cdot\theta_k\mathrm{d}\Omega. \quad (11)$$

The combining of equations, and gives the final form of the $M\theta$ integral:

$$M\theta=\frac{1}{2}\int_{\Omega}\left(\sigma_{ij}^{(u)}\cdot v_{i,k}-\sigma_{ij,k}^{(v)}\cdot u_i\right)\cdot\theta_{k,j}\mathrm{d}\Omega+\frac{1}{2}\int_{\Omega}\left(\left(\sigma_{ij}^{(v)}\cdot(u_{i,j})_{,k}+\sigma_{ij}^{(u)}\cdot(v_{i,j})_{,k}\right)-\left(\left(\sigma_{ij}^{(v)}\cdot u_{i,j}\right)_{,k}+\left(\sigma_{ij}^{(u)}\cdot v_{i,j}\right)_{,k}\right)\right)\cdot\theta_k\mathrm{d}\Omega. \quad (12)$$

The first term of expression translates the modeling approach for stationary cracking. The second term introduces the modeling form for the crack growth process (Moutou Pitti et al., 2007b).

3. Viscoelastic generalization and physical interpretation

3.1. Viscoelastic generalization of M-integral

The introduction of viscoelastic behavior is due to the generalized Kelvin Voigt model, composed of N cells of Kelvin Voigt for differed response and one specific spring for elastic and instantaneous response. (Fig. 3).

Then, equation can be generalized by the following expression:

$$M=\frac{1}{2}\int_{\Gamma_1}\left({}^{p}\sigma_{ij,1}^{(v)}\cdot u_i^p-{}^{p}\sigma_{ij}^{(u)}\cdot v_{i,j}^p\right)\cdot n_j\mathrm{d}\Gamma_1+\frac{1}{2}\int_{A(\Gamma_1)}\left(\left({}^{p}\sigma_{ij}^{(v)}\cdot(u_{i,j}^p)_{,1}+{}^{p}\sigma_{ij}^{u}\cdot(v_{i,j}^p)_{,1}\right)-\left(\left({}^{p}\sigma_{ij}^{v}\cdot u_{i,j}^p\right)_{,1}+\left({}^{p}\sigma_{ij}^{u}\cdot v_{i,j}^p\right)_{,1}\right)\right)\mathrm{d}V. \quad (13)$$

Employing ${}^{p}\sigma_{ij}^{(u)}$ and ${}^{p}\sigma_{ij}^{(v)}$ as real and virtual stress components in the pth spring and introducing equivalent real (u_i^p) and virtual (v_i^p) displacements of the complex pth Kelvin Voigt cell, respectively, the $M\theta$ form of expression (12) becomes:

$$M\theta_v^p=\frac{1}{2}\int_{\Omega}{}^{p}\left(\sigma_{ij}^{(v)}\cdot v_{i,k}^p-{}^{p}\sigma_{ij,k}^{(u)}\cdot u_i^p\right)\cdot\theta_{k,j}\mathrm{d}V+\frac{1}{2}\int_{\Omega}\left(\left({}^{p}\sigma_{ij}^{(v)}\cdot\left(u_{i,j}^p\right)_{,k}+{}^{p}\sigma_{ij}^{(u)}\cdot\left(v_{i,j}^p\right)_{,k}\right)-\left(\left({}^{p}\sigma_{ij}^{(v)}\cdot u_{i,j}^p\right)_{,k}+\left({}^{p}\sigma_{ij}^{(u)}\cdot v_{i,j}^p\right)_{,k}\right)\right)\cdot\theta_k\mathrm{d}\quad\text{with } p=(0,1,\ldots,N). \quad (14)$$

3.2. Physical interpretation of M-integral

According to the definition of the energy release rate G, the superposition principle gives (Moutou Pitti et al., 2007a; Dubois et al., 1999):

$$M\theta_v^p=C_1^p\cdot\frac{{}^{u}K_I^p\cdot{}^{v}K_I^p}{8}+C_2^p\cdot\frac{{}^{u}K_{II}^p\cdot{}^{v}K_{II}^p}{8}. \quad (15)$$

${}^{u}K_I^p$ and ${}^{u}K_{II}^p$ are the real stress intensity factors in mode I and mode II, respectively. C_1^p and C_2^p designate the reduced viscoelastic compliances in opening and shear modes, respectively (Valentin and Morlier, 1982). Their form is given by the following:

$$C_1^p=4\cdot\Re e\left[i\cdot\frac{q_2^p\cdot s_1^p-q_1^p\cdot s_2^p}{s_1^p-s_2^p}\right]\cdot\text{ and }C_2^p=4\cdot\Re e\left[i\cdot\frac{p_2^p-p_1^p}{s_1^p-s_2^p}\right]. \quad (16)$$

Each virtual stress and displacement field induces virtual stress intensity factors, denoted ${}^{v}K_I^p$ and ${}^{v}K_{II}^p$ for each fracture mode, respectively. The perfect separating mixed-mode fracture is given by performing two distinct calculations and choosing judicious values of the corresponding virtual stress intensity factors, for example (Moutou Pitti et al., 2007a):

$${}^{u}K_I^p=\frac{8\cdot M\theta_v^p\left({}^{v}K_I^p=1,{}^{v}K_{II}^p=0\right)}{C_1^p}\text{ and }{}^{u}K_{II}^p=\frac{8\cdot M\theta_v^p\left({}^{v}K_I^p=0,{}^{v}K_{II}^p=1\right)}{C_2^p}. \quad (17)$$

From expressions (14), (15) and (17), the viscoelastic energy release rate G_v^p is given by:

$$G_v^p={}^{1}G_v^p+{}^{2}G_v^p\text{ with }{}^{1}G_v^p=C_1^p\frac{\left({}^{u}K_I^p\right)^2}{8}\text{ and }{}^{2}G_v^p=C_2^p\frac{\left({}^{u}K_{II}^p\right)^2}{8}. \quad (18)$$

${}^{1}G_v^p$ and ${}^{2}G_v^p$ represent the energy release rate contribution induced by the free energy stored in the pth spring for opening and shear modes, respectively. Finally, the total partition of the energy release rate is given by the following summation:

$$Gv1=\sum_k{}^{1}G_v^p\text{ and }Gv2=\sum_k{}^{2}G_v^p\text{ with }p=(0,1\ldots,N). \quad (19)$$

4. Finite element process and crack growth algorithm

4.1. Finite element computation

In order to evaluate mechanical fields and use the energy balance in the time domain, a finite element method is preferred. The linear viscoelastic behavior can be expressed with a discrete spectrum representation of each creep function component (Ghazlan et al., 1995). For viscoelastic material, the relationship connecting strain ε_{ij} and stress σ_{kl} is given by the Boltzmann equation:

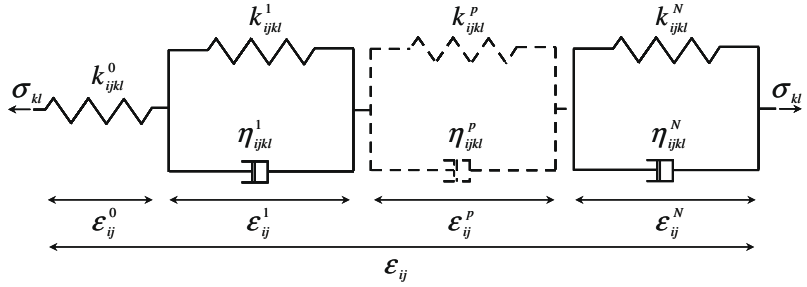

Fig. 3. Generalized Kelvin Voigt model.

$$\varepsilon_{ij}(t) = \int_0^t J_{ijkl}(t-\tau)\cdot\frac{\partial\sigma_{kl}}{\partial\tau}\mathrm{d}\tau. \tag{20}$$

$J_{ijkl}(t)$ are components of the four order creep compliance tensor described with spring rigidities $k^p_{ijkl}(p\in\{0;1;\ldots;N\})$ and dash-pot viscosities $\eta^m_{ijkl}(m\in\{1;\ldots;N\})$ such that

$$J_{ijkl}(t) = \frac{1}{k^o_{ijkl}} + \sum_{m=1}^{N}\frac{1}{k^m_{ijkl}}\cdot\left(1-\exp^{-\lambda^m_{ijkl}\cdot t}\right) \text{ with } \lambda^m_{ijkl} = \frac{k^m_{ijkl}}{\eta^m_{ijkl}}. \tag{21}$$

In the Kelvin Voigt generalized mode (Fig. 3), the total partition of the strain tensor is translated as

$$\varepsilon_{ij} = \sum_{k,l}\Pi_{ijkl} \text{ with } \Pi_{ijkl} = \Pi^{(0)}_{ijkl} + \sum_{m=1}^{N}\Pi^{(m)}_{ijkl} \quad m=(1,\ldots,N). \tag{22}$$

Here, $\Pi_{ijkl}(t_n)$ represents the part of the strain component generated by the stress component $\sigma_{kl}(t_n)$. Then, the governing equations can be obtained using finite difference integration and a step-by-step process. This method allows to resolve, in the time domain, the hereditary behavior (20) without retaining the complete past history of the stress tensor. According to the superposition principle, the incremental constitutive equation using a linear approximation of stress in each time step $\Delta t_n = t_n - t_{n-1}$ is given by (Ghazlan et al., 1995; Moutou Pitti et al., 2007a):

$$\Delta\varepsilon_{ij}(t_n) = \Psi_{ijkl}\cdot\Delta\sigma_{kl}(t_n) + \tilde{\varepsilon}_{ij}(t_{n-1}). \tag{23}$$

The terms $\Delta\varepsilon_{ij}(t_n)$ and $\Delta\sigma_{kl}(t_n)$ designate the strain and stress increments during the time increment Δt_n.$\tilde{\varepsilon}_{ij}(t_{n-1})$ represents the global influences of the mechanical history. Ψ_{ijkl} translates the equivalent compliance function. Its form is given by:

$$\Psi_{ijkl} = \frac{1}{k^0_{ijkl}} + \sum_{m=1}^{N}\frac{1}{k^m_{ijkl}}\cdot\left(1-\frac{1-\exp^{-\lambda^m_{ijkl}\cdot\Delta t_n}}{\lambda^m_{ijkl}\cdot\Delta t_n}\right) \text{ with } \lambda^m_{ijkl} = \frac{k^m_{ijkl}}{\eta^m_{ijkl}}. \tag{24}$$

Introducing the creep function form in the definition of the free energy density (Dubois and Petit, 2005), F can be rewritten as:

$$F = \frac{1}{2}\cdot k^0_{ijkl}\cdot\varepsilon^0_{ij}\cdot\varepsilon^0_{kl} + \sum_{m=1}^{N}\frac{1}{2}\cdot k^m_{ijkl}\cdot\varepsilon^m_{ij}\cdot\varepsilon^m_{kl}, \tag{25}$$

$$\text{with } \varepsilon^0_{ij} = \frac{1}{k^0_{ijkl}}\cdot\sigma_{kl} \text{ and } \varepsilon^m_{ij} = \int_{0^-}^{t}\frac{1}{k^0_{ijkl}}\cdot\left(1-\exp^{-\lambda^m_{ijkl}\cdot(t-\tau)}\right)\cdot\frac{\partial\sigma_{kl}}{\partial\tau}\mathrm{d}\tau. \tag{26}$$

In the time domain, the evaluation of $F(t_n)$, or Eq. (25), requires the computation of the increments $\Delta\varepsilon^0_{ij}(t_n)$ and $\Delta\varepsilon^m_{ij}(t_n)$. With relations (26), these increments may be noted as follows:

$$\Delta\varepsilon^0_{ij}(t_n) = \frac{1}{k^0_{ijkl}}\cdot\Delta\sigma_{kl}(t_n) \text{ and } \Delta\varepsilon^m_{ij}(t_n) = \sum_{k,l}\Delta\Pi^m_{ijkl}(t_n), \tag{27}$$

where $\Delta\Pi_{ijkl}(t_n)$ is the increment of $\Pi_{ijkl}(t_n)$ and is written as

$$\Delta\Pi^m_{ijkl}(t_n) = \left(\exp^{-\lambda^m_{ijkl}\cdot\Delta t_n}-1\right)\cdot\Pi^m_{ijkl}(t_{n-1}) + \left(\frac{1-\exp^{-\lambda^m_{ijkl}\cdot\Delta t_n}}{k^m_{ijkl}}\right)\cdot\sigma_{kl}(t_{n-1}) + \frac{1}{k^m_{ijkl}}\cdot\left(1-\frac{1-\exp^{-\lambda^m_{ijkl}\cdot\Delta t_n}}{\lambda^m_{ijkl}\cdot\Delta t_n}\right)\cdot\Delta\sigma_{kl}(t_n). \tag{28}$$

The incremental formulation is resolved with a finite element method by using a nodal displacement vector increment $\{\Delta u^p\}(t_n)$ in the following balance equation (Ghazlan et al., 1995; Chazal and Dubois, 2001):

$$K^p_T\cdot\{\Delta u^p\}(t_n) = \{\Delta F^p_{ext}\}(t_n) + \{\widetilde{F}^p\}(t_{n-1}). \tag{29}$$

K^p_T is the tangent matrix defined with the Jacobean matrix B and the equivalent compliance tensor $[\Psi]$ by

$$K^p_T = \int_\Omega B^T\cdot[\Psi^p]^{-1}\cdot B\mathrm{d}\Omega. \tag{30}$$

$\{\Delta F^p_{ext}\}(t_n)$ represents the increment of the nodal force vector induced by external increment loading. $\{\widetilde{F}^p\}(t_{n-1})$ is the supplementary viscous load vector representing the complete mechanical history. It is given by

$$\{\widetilde{F}^p\}(t_{n-1}) = \int_\Omega B^T\cdot\Psi^p\cdot\{\tilde{\varepsilon}^p\}(t_{n-1})\mathrm{d}\Omega, \tag{31}$$

where $\{\tilde{\varepsilon}^p\}(t_{n-1})$is the strain vector, defined for each integration point.

4.2. Viscoelastic crack growth algorithm

For mixed-mode crack problems, the loading and geometry symmetries are affected by the extent of the advancing crack tip. In this case, a re-meshing of the numerical model is necessary after each crack tip advance. To overcome this difficulty, hereditary mechanical fields have been projected in the transformed mesh. This complex algorithm must separate the time and geometry variations (see Fig. 4).

First, all mechanical fields and the crack length a are supposed to be known at time t_n. That way, the stress and external loading, $\sigma_i(t_n)$ and $F_i(t_n)$, respectively, are defined in the initial mesh W_i and characterized by a crack length a (step 0).

Second, the instantaneous crack tip advance Δa is fixed; the new mesh denoted W_{i+1} is found by re-meshing. The stress $\sigma_{i+1}(t_n)$ is computed with this new geometry. We define $\sigma^p_i(t_n)$ to be the geometric projection of $\sigma_i(t_n)$ on the mesh W_{i+1}. The induced perturbation field can be defined as follows: $\Delta\sigma_i(t_n) = \sigma_{i+1}(t_n) - \sigma^p_i(t_n)$.

Third, $-\Delta\sigma_i(t_n)$ is applied as a cohesion stress (equivalent external loading) by using the superposition principle. This supplementary loading allows for closing the new crack on Δa. In this case, we obtain an equivalent configuration between steps 0 and 3 (the same mechanical state) with two different meshes. $\Delta\sigma_i$ can be interpreted as the stress cohesion in a process zone around the crack tip (Schapery, 1984).

Fourth, the crack length advance is fixed, and viscoelastic procedures are allowed to operate. The stress cohesion $\Delta\sigma_i$ is employed in the viscoelastic incremental procedure as an external load vector during the time increment Δt_n (see Eq. (29)), inducing a non cohesion of crack lips as the crack propagates in time. In the time domain, viscoelastic mechanic fields are obtained.

Fifth, the virtual procedure and $M\theta$ procedure are applied in order to calculate fracture parameters.

5. Numerical validations

In this last section, we present numerical simulations which prove the non path dependence of the M-integral on hereditary behavior and discuss the crack growth process over time. In recent works, Moutou Pitti et al. (2007a) have shown that this approach is valid for a stationary crack. Now, we propose to generalize the validation by imposing a time dependent crack tip advance according to the numerical algorithm presented in Fig. 4.

5.1. CTS specimen and mechanical properties

The numerical simulation requires a specific specimen on which to impose different mixed-mode ratios, orthotropic properties and viscoelastic behaviors. According to certain specifications, we have opted for a Constant Tension Shear initially developed by Richard

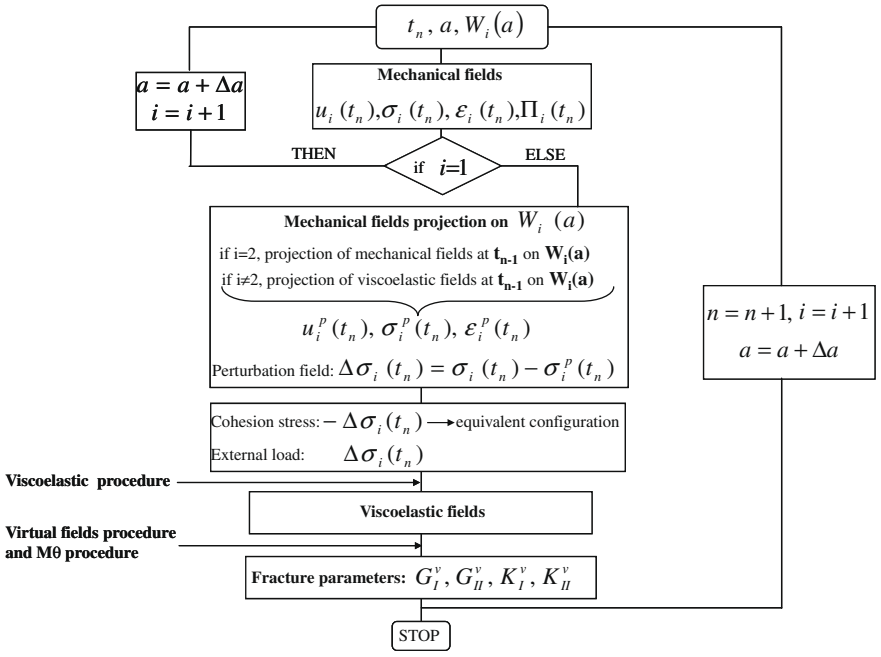

Fig. 4. Viscoelastic crack growth algorithm.

(Richard, 1981; Richard and Benitz, 1983) in order to obtain mixed-mode configurations in isotropic and ductile materials (Zhang et al., 2006; Ma et al., 2006). In order to take into account orthotropic assumptions, Valentin and Caumes (1989) have adapted the geometry to orthotropic materials such as wood. Steel Arcan enables us to impose different mixed-mode ratios. In Fig. 5, the loading points A_α and B_α with $\alpha \in (1 \ldots, 7)$ are oriented according to the angle β. The pure mode I is obtained by using opposite forces in A_1 and B_1 with $\beta = 0°$. In the same way, loading points A_7 and B_7 (with $\beta = 90°$) are employed in order to impose a pure shear mode. Intermediate positions induce different mixed-mode ratios.

The simulations integrate orthotropic viscoelastic behavior for long term loadings. We propose to choose a spine spruce specimen characterized by a four order creep tensor. Experimental identification challenges us to choose a simplified and proportional creep tensor, defined as follows:

$$J(t) = f(t) \cdot C_0. \tag{32}$$

$f(t)$ is a creep function. C_0 is an unitary constant compliance tensor that can take this form:

$$C_0 = \begin{bmatrix} 1 & -\upsilon & 0 \\ -\upsilon & \frac{E_X}{E_Y} & 0 \\ 0 & 0 & \frac{E_X}{G_{XY}} \end{bmatrix}. \tag{33}$$

E_Y and G_{XY} are the transverse and shear modulus, respectively, and υ is Poisson's ratio in the XY plane. For the simulations, these properties are fixed according to the characteristics of pine spruce (Dubois et al., 2001):

$$E_X = 15{,}000\ \text{MPa}, \quad E_Y = 600\ \text{MPa}, \quad G_{XY} = 700\ \text{MPa}, \quad \text{and } \upsilon = 0{,}4. \tag{34}$$

The creep function $f(t)$ has been interpolated by Dubois et al. (2001) using a crack opening displacement method on a Double Cantilever Beam specimen. According to long time simulations, we have opted for a creep interpolation requiring six Kelvin Voigt cells. Each characteristic time is defined by the spectrum decomposition. In these conditions, the creep function is given, in MPa^{-1}, by:

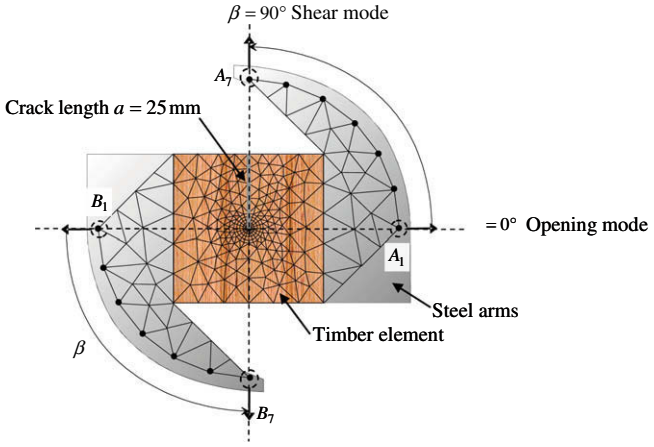

Fig. 5. CTS (Constant Tension Shear) specimen.

$$f(t) = 6.7 \cdot 10^{-7} \cdot \begin{bmatrix} 100 + 1.35 \cdot (1 - e^{-22t}) + 1.34 \cdot (1 - e^{-2.2t}) \\ +4.37 \cdot (1 - e^{-2.2 \cdot 10^{-1} t}) + 3.62 \cdot (1 - e^{-2.2 \cdot 10^{-2} t}) \\ +12.8 \cdot (1 - e^{-2.2 \cdot 10^{-3} t}) + 31.0 \cdot (1 - e^{-2.2 \cdot 10^{-4} t}) \end{bmatrix}. \tag{35}$$

5.2. Finite element mesh

The finite element mesh is shown in Fig. 5. The asymmetry of the loading requires a total geometry discretization. In order to show the non-dependence of the integration domain for the M-integral, we opt for a circular mesh around the crack tip composed of seven crowns (C0, C2, C4, C6, C8, C10, C12, see Fig. 6). The integration domain is defined by the $\vec{\theta}$ vector in which each component is treated as a field gradient in each crown.

5.3. The insensitivity of the M-integral to the integration domain

The first application deals with the insensitivity of the M-integral to the integration domain during crack growth process. The

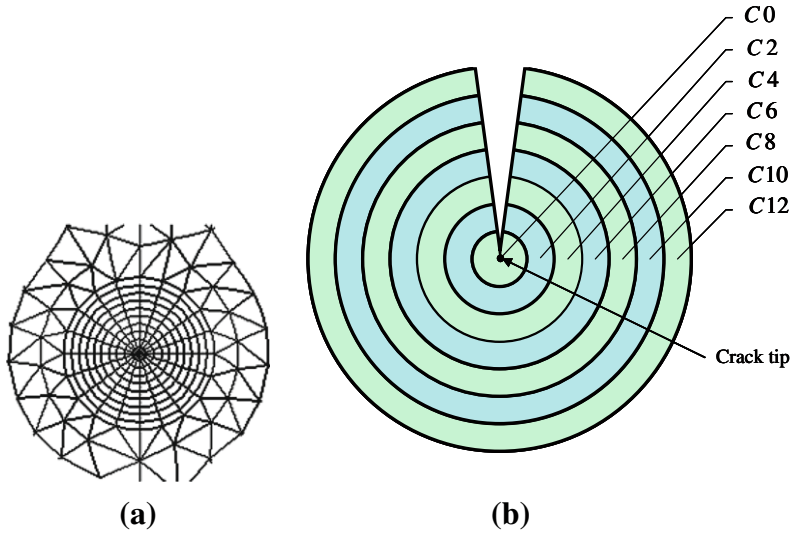

Fig. 6. (a) numerical mesh around the crack tip and (b) crowns around the crack tip.

simulation starts with an initial crack length of 25 mm. The slow crack tip speed is fixed to 7×10^{-5} mm/min. We stop the process at a final crack length of 30 mm. During the crack growth process, the energy release rate is computed using different integration crowns. The M integral is employed by uncoupling part of open mode $G\upsilon 1$ and part of shear mode $G\upsilon 2$. Three mixed-mode configurations have been studied, pure mode I ($\beta = 0^\circ$), pure mode II ($\beta = 90^\circ$) and mixed mode ($\beta = 45^\circ$). The mechanical loading is imposed by two unitary opposite forces.

Figs. 7 and 8 show the final values for $G\upsilon 1$ and $G\upsilon 2$ at the final crack length (30 mm). Crowns C2 and C4 are in the singular field region for which the M-integral results give evidence of numerical perturbations. However, if we integrate far mechanical fields (crowns C6 to C12), the results show relative stability with an average error of 5%. In this context, we can conclude that the global algorithm of mixed mode uncoupling during the crack growth process is validated.

5.4. Energy release rate versus crack tip speed

A second numerical application deals with the variation of energy release rate versus the crack growth speed during creep loadings. The initial crack length is 24 mm. Four successive cracks in increments of 8 mm have been simulated up to a final crack length of 62 mm. We operate a crack growth simulation by imposing different values for the crack growth speed as characterized by a specific time increment during each step of the crack tip advance. In order to examine the uncoupling process, we limit the simulation to a mixed-mode configuration ($\beta = 45^\circ$). According to past simulations, the loading is constant with unitary opposing forces. The computation is performed using integration crown C6. The time increment 0 represents an elastic or instantaneous crack growth process. Part of the open mode is presented in Fig. 9 in terms of energy release rate versus time increment. The same representation, in terms of shear mode, is presented in Fig. 10. These results show

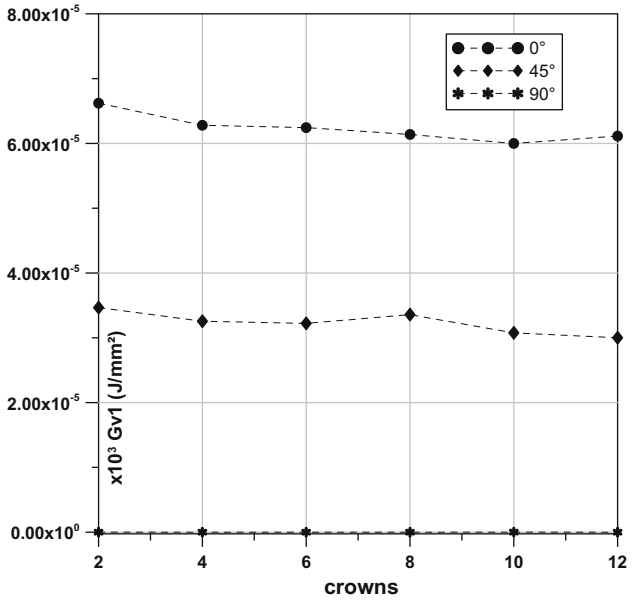

Fig. 7. Energy release rate $G\upsilon 1$ versus integration crown.

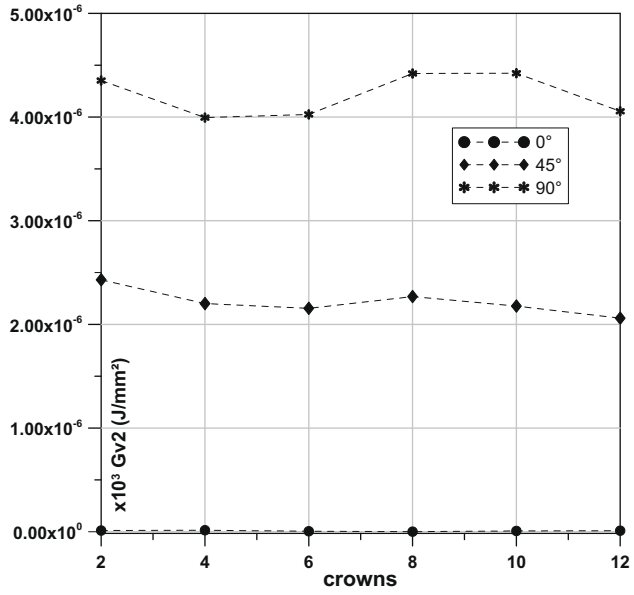

Fig. 8. Energy release rate $G\upsilon 2$ versus integration crown.

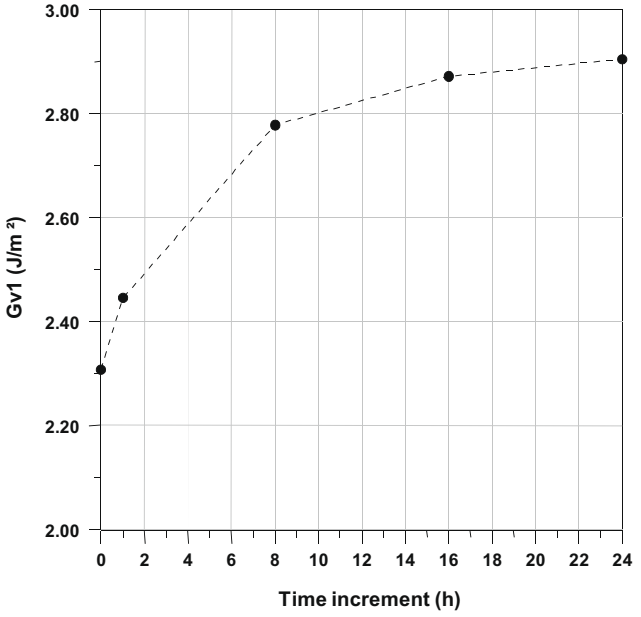

Fig. 9. Energy release rate $Gv1$ versus time in mixed mode 45° (part of opening mode).

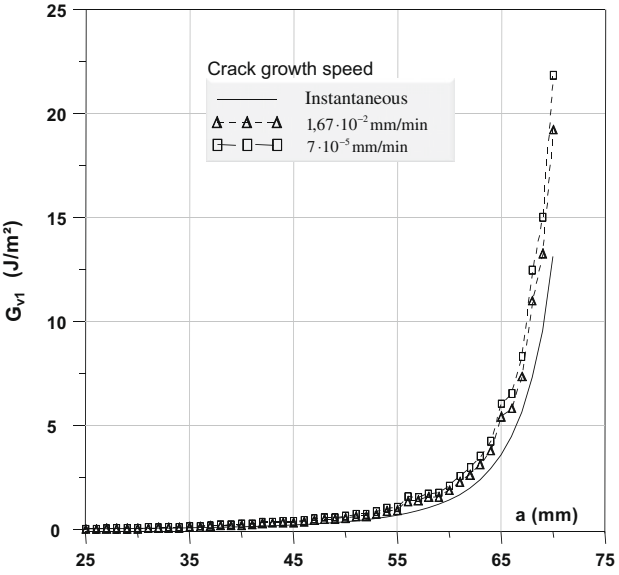

Fig. 11. Energy release rate $Gv1$ versus crack length and crack growth speed (part of opening mode).

the importance of the viscoelasticity in the creep crack growth process in a progressive incohesion of crack lips.

A last simulation deals with the influence of the crack speed on the apparent energy release rate versus the crack tip position. In this case, the crack increment is 1 mm and we impose three different speeds (instantaneous response, 1.67×10^{-2} mm/min and 7×10^{-5} mm/min). In the following results, crown C6 was chosen and the crack increment was set to be 1 mm. Figs. 11 and 12 show the evolutions of $Gv1$ and $Gv2$ in mixed mode ($\beta = 45°$) versus crack length. These results show the continuous crack lip incohesion in the process zone caused by the relaxation time induced by viscoelastic effects. However, if this simulation gives evidence of the energy release rate evolution versus crack speed, it is characterized by a constant stress field distribution. In this case, we can conclude that stress intensity factors must only be dependent on the crack length, and not on time. This fact is proved in Figs. 13 and 14, and it validates the crack growth algorithm and the M-integral response.

6. Conclusions

An analytical formulation of the M-integral separating mixed-mode fractures in viscoelastic media during the creep crack growth process has been proposed. Using the generalized Kelvin Voigt model, this approach has been generalized to include viscoelastic behavior. In order to implement the M-integral in finite element software, a complex algorithm uncoupling viscoelastic incremental formulations and fracture procedures has been developed. In numerical process, the mixed-mode ratios have been reproduced by the CTS specimen. Then, the insensitivity of the M-integral to the integration domain has been proven by the stability of energy

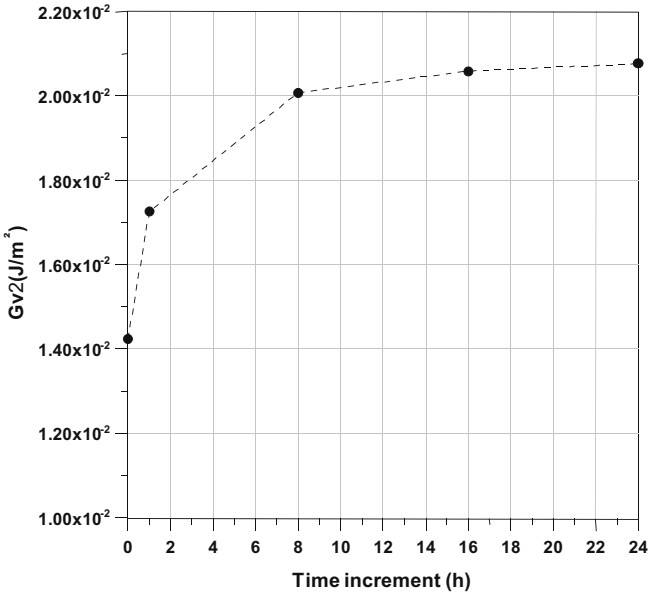

Fig. 10. Energy release rate $Gv2$ versus time in mixed mode 45° (part of shear mode).

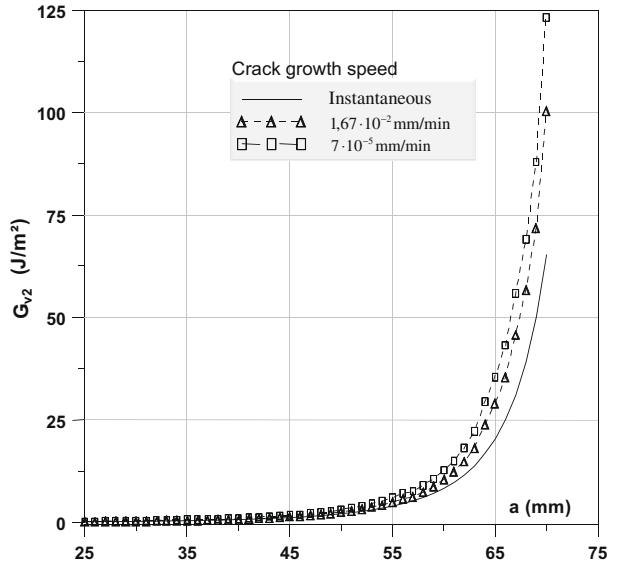

Fig. 12. Energy release rate $Gv2$ versus crack length and crack growth speed (part of shear mode).

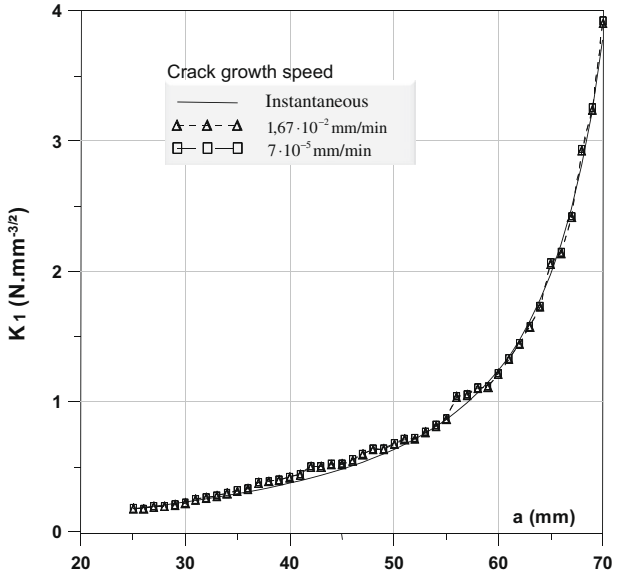

Fig. 13. Stress intensity factor K1 versus crack length and crack growth speed.

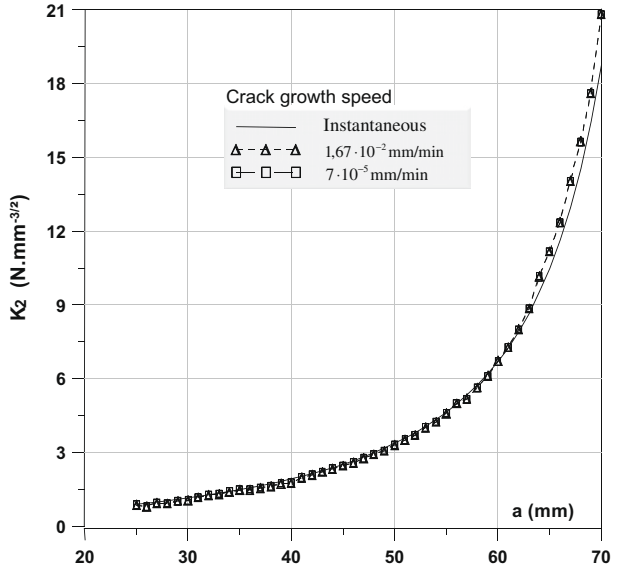

Fig. 14. Stress intensity factor K2 versus crack length and crack growth speed.

release rate Gv versus different crowns. Also the variations of Gv have been determined as a function of time and crack length in the mixed mode of 45°. Finally, this numerical approach is validated according to a stability of stress intensity factors versus crack growth speed. So, this work requests experimental validation.

References

Barbero, E.J., Luciano, R., 1995. Micromechanical formulas for the relaxation tensor of linear viscoelastic composites with transversely isotropic fibers. International Journal of Solids and Structures 32 (13), 1859–1872.

Bian, L.C., Lim, J.K., 2007. Material plasticity dependence of mixed mode fatigue crack growth in commonly used engineering materials. International Journal of Solids and Structures 44, 8440–8456.

Destuynder, P., Djaoua, M., Lescure, S., 1983. Quelques remarques sur la mécanique de la rupture élastique. Journal de Mécanique Théorique et Appliquée 2, 113–135.

Dubois, F., Chazal, C., Petit, C., 1999. Modelling of crack growth initiation in a linear viscoelastic material. Journal of Theoretical and Applied Mechanics 37, 207–222.

Dubois, F., Chazal, C., Petit, C., 2001. Viscoelastic crack growth process in wood timbers: an approach by the finite element method for mode I fracture. International Journal of Fracture 113, 367–388.

Dubois, F., Petit, C., 2005. Modelling of the crack growth initiation in viscoelastic media by the $G\theta v$-integral. Engineering Fracture Mechanics 72, 2821–2836.

Chazal, C., Dubois, F., 2001. A new incremental formulation in the time domain of crack initiation in an orthotropic linearly viscoelastic solid. Mechanics of Time-Dependent Materials 5, 3–21.

Chen, F.M.K., Shield, R.T., 1977. Conservation laws in elasticity of the J-integral type. Journal of Applied Mechanics and Physics 28, 1–22.

Cortés, F., Elejabarrieta, M.J., 2006. Modelling viscoelastic materials whose storage modulus is constant with frequency. International Journal of Solids and Structures 43, 7221–7226.

Ghazlan, G., Caperaa, S., Petit, C., 1995. An incremental formulation for the linear analysis of thin viscoelastic structures using generalized variables. International Journal of Numerical Methods Engineering 38, 3315–3333.

Ma, S., Zhang, X.B., Recho, N., Li, J., 2006. The mixed-mode investigation of the fatigue crack in CTS metallic specimen. International Journal of Fatigue 28, 1780–1790.

Moutou Pitti, R., Dubois, F., Petit, C., Sauvat, N., 2006. Fracture of wood under mixed mode loading: numerical approach by the $M\theta v$-integral. In: Proceedings of Ninth Word Conference of Timber Engineering. Portland.

Moutou Pitti, R., Dubois, F., Petit, C., Sauvat, N., 2007a. Mixed mode fracture separation in viscoelastic orthotropic media: numerical and analytical approach by the $M\theta v$-integral. International Journal of Fracture 145, 181–193.

Moutou Pitti, R., Dubois, F., Pop, C., Sauvat, N., Petit, C., 2007b. Mv-integral for the crack growth in a viscoelastic media. Comptes Rendus Mécanique 335, 727–731.

Noether, E., 1971. Invariant variations problem. Transport Theory Statistical Physics 1, 183–207.

Ratnesh, Khandelwal, Chandra Kishen, J.M., 2008. The use of conservative integral in bi-material interface crack problems subjected to thermal loads. International Journal of Solids and Structures 45, 2976–2992.

Rice, JR., 1968. A path independent integral and the approximate analysis of strain concentration by notches and cracks. Journal of Applied Mechanics 35, 379–385.

Richard, HA., 1981. A new compact shear specimen. International Journal of Fracture 17, 105–107.

Richard, HA., Benitz, K., 1983. A loading device for the creation of mixed mode in fracture mechanics. International Journal of Fracture 22, R55–R58.

Schapery, R.A., 1984. Correspondence principles and a generalized J integral for large deformation and fracture analysis of viscoelastic media. International Journal of Fracture 25, 195–223.

Sih, G.C., 1974. Strain energy factor applied to mixed mode crack problems. International Journal of Fracture 10, 305–321.

Sun, C.T., Qian, W., 1997. The use of finite extension strain energy release rates in fracture of interfacial cracks. International Journal of Solids and Structure 34, 2595–2609.

Tenchev, R.T., Falzon, BG., 2007. A correction to the analytical solution of the mixed-mode bending (MMB) problem. Composites Science and Technology 67, 662–668.

Valentin, G., Caumes, P., 1989. Crack propagation in mixed mode in wood: a new specimen. Wood Science and Technology 23, 43–53.

Valentin, G., Morlier, P., 1982. A criterion of crack propagation in timber. Matériaux et Constructions 88, 291–298.

Vasic, S., Smith, I., Landis, E., 2005. Finite element techniques for models for wood fracture mechanics. Wood Science and Technology 39, 3–17.

Zhang, X.B., Ma, S., Recho, N., Li, J., 2006. Bifurcation and propagation of a mixed-mode crack in ductile material. Engineering Fracture Mechanics 3, 1925–1939.